Article:
Sokkar, T.Z.N., El-Bakary, M.A., Raslan, M.I. et al. (2 more authors) (2019) Interferometric investigation of the opto-mechanical and structural properties of iPP/TiO2 nanocomposite fibers. Microscopy Research & Technique. ISSN 1059-910X

https://doi.org/10.1002/jemt.23212

Interferometric investigation of the opto-mechanical and structural properties of PP/TiO_2 nanocomposite fibres

T.Z.N. Sokkar[1], M.A. El-Bakary[1*], M.I. Raslan[2], N.A. Al-Kalali[3], H.M. El-Dessouky[1,4]

[1] Department of Physics, Faculty of Science, Mansoura University, Mansoura, Egypt

[2] Faculty of Oral and Dental Medicine, Delta University, Gamasa, Egypt

[3] Department of Physics, Faculty of Science, Hadhramout University, Mukalla, Yemen

[4] Composite Centre, AMRC with Boeing, University of Sheffield, Rotherham, UK

*Corresponding author e-mail address: elbakary2@yahoo.com (M. A. El-Bakary)

Abstract

Fibres that missing specific features and functionalities could be innovated and functionalised via nanoadditives, in particular metal oxides. Titanium oxide (TiO_2) nanoparticles have been added to isotactic polypropylene (iPP) to form iPP/TiO_2 nanocomposite fibres. Three samples of iPP/TiO_2 fibres were extruded at three extrusion speeds 25, 50, and 78m/min were considered in this study. Mach–Zehnder interferometer was used to assess the changes in the opto-mechanical and geometrical parameters of iPP/TiO_2 nanocomposite fibres along the fibre axis. The mechanical drawing device along with Mach–Zehnder interferometer was utilised to stretch the filaments to different draw ratios. The effect of mechanical cold drawing and extrusion speed on the optical and physical characteristics of iPP/TiO_2 nanocomposite fibres were determined along the fibre axis. The optical and physical variation along the nanocomposite samples were characterised by measuring their refractive indices, birefringence, refractive index profile along the fibre axis. The diffraction of a He–Ne laser beam was used to define the variation of the fibre diameter along the fibre axis through their cross-sectional area and shape. A sample of uniform diameter from neat iPP fibres was used as a reference material for studying the variation of the iPP/TiO_2 fibre diameter along the fibre axis. As a result, the iPP/TiO_2 nanocomposite fibres exhibited non-uniform diameters. The dispersion of TiO_2 particles in nanocomposite fibres influences the properties' consistency along and across the fibre.

Keywords

Polypropylene fibres. Nanocomposites. Interferometry. Cold drawing. Birefringence.

1. Introduction

In recent years, polymer-nanoparticle composites have attracted the interest of many researchers due to their great potential as multifunctional materials for a wide variety of applications. In textile fibres, nanoparticle additives such as TiO_2, ZnO, Ag, and carbon nanotubes enhance fabric characteristics such as self-cleaning, high tensile strength, durability, conductivity, anti-bacterial, anti-static and UV-protection [1]. Polymer nanocomposites are derived by incorporating nanoparticles into a bulk polymer. The resulting composite materials often exhibited extraordinarily and interesting properties compared to the bulk (base) material [2-4].

Titanium oxide (TiO_2) is one of the popular industrial and engineering material in our daily life because of its efficiency in scattering visible light and having a high refractive index. For many years, TiO_2 has been used as a delustrant in synthetic fibres imparting whiteness and brightness as a white pigment. It has high opacity when incorporated into a plastic formulation. When developing TiO_2 into nanoparticles, it has large total surface area per unit volume that makes it has the opportunity to exploit unique optical, electrical and chemical attributes when incorporated into synthetic fibres. Also, Nano sized TiO_2 should give enhanced UV protection by scattering UV rays through its high refractive index and by absorbing UV rays because of its semiconductor properties [1, 5, 6].

Isotactic polypropylene (iPP) fibres is one of the most widely used in textile industry. It has many features like ease of processing, low density and high tensile strength. It can be used in numerous applications such as woven fabrics, nonwovens, geotextiles, industrial packaging bags, sanitary napkins, medical textiles, etc. However, it suffers from the disadvantages which limit its end use areas [7,8]. The iPP/TiO_2 nanocomposites can be manufactured by the incorporation of TiO_2 nanoparticles into the iPP matrix through melting spinning process. The obtained nanocomposites have superior mechanical and thermal properties compared to the conventional polypropylene [5, 9, 10].

Interferometry is an optical technique that can be trustily used for characterising fibres and determining their properties. There are various interferometric methods have been designed and utilised to study the opto-mechanical and physical properties of natural and synthetic fibres [11]. Mach–Zehnder interferometer has been utilised to measure the refractive indices ($n^{\parallel}$ and

$n^{\perp}$) and birefringence of polymeric fibres [12]. Such optical parameters were used to study the microstructure of fibres, in particular the internal molecular arrangement inside fibres [13].

The measurement of birefringence provides a rapid and powerful approach for studying the structural properties such as molecular orientation and anisotropic properties of polymeric fibres [11]. The drawn (oriented) fibres reveal the transverse birefringence gradients in optical anisotropy when both refractive indices ($n^{\parallel}$ and $n^{\perp}$) are measured at the marginal and central zones of the fibre. Measurements of the refractive index and birefringence profiles are considered to be one of the interesting properties suggested as a quality control during the manufacturing of textile fibres [14]. The drawing process of fibres provides optimal alignment of the molecular chain along the fibre axis. The degree of orientation might vary significantly from one fibre to another, depending on the fibre history throughout spinning and consequent processes such as hot drawing. The phenomenon of cold drawing is common to both amorphous and semi-crystalline polymers [15].

In this work the effect of mechanical cold drawing and extrusion speed on the molecular orientation and physical structure parameters of iPP/TiO_2 nanocomposite fibres is optically investigated. The mechanical drawing device linked with Mach–Zehnder interferometer is used to stretch the iPP/TiO_2 nanocomposite fibres to different draw ratios at a constant drawing rate. The molecular structure of the drawn iPP/TiO_2 fibres is characterised through refractive indices, birefringence and refractive index profile measurements. The relationships between the physical and optical parameters at different drawing conditions are suggested. Microinterferograms are presented for illustration.

2. Materials

Three different samples of nanocomposite monofilament fibres, iPP/ TiO_2, have isotactic polypropylene (iPP) as a bulk material or matrix polymer and titanium oxide nanoparticles, (TiO_2) as additives to constitute iPP/ TiO_2 nanocomposites. These samples were produced as spun using a 10mm twin-screw extruder at the Centre for Technical Textiles, School of Design, University of Leeds, UK [1]. The nanocomposite samples contain 2% TiO_2 dispersed in the iPP and spun at three extrusion speeds 25m/min, 50m/min and 78m/min. The average diameters of the three extracted samples and the take-up velocity are given in table (1).

3. Experimental technique

The experimental setup of Mach-Zehnder interferometer is shown in Figure (1)**.** It consists of a He–Ne laser source generates a monochromatic light beam of wavelength λ=632.8 nm, spatial filter (S), a polarizer (P), two identical beam splitters (BS1, BS2), two identical mirrors (M1, M2), object stage (OS), microscope objective (MO), and a CCD camera. The fibre sample is immersed in a suitable immersion oil. A mechanical drawing device (SD) attached with the Mach-Zehnder interferometer arrangement to detect mechanical deformation of iPP/TiO_2 nanocomposite fibres during the cold drawing process. During the cold drawing the microinterfergrams recorded and stored via CCD. An image analysis was carried out to conduct the phase map from microinterferogram using MAT Lab environment. From which the refractive indices and birefringence are calculated.

4. Results and discussions

Laser diffraction is a common technique for rapid determination of the fibres diameter. The analysis of diffraction pattern, produced by the incidence of a laser beam on a fibre sample, is performed according to references [16, 17]. The diameter of tested fibre (d) is determined using the following equation.

$$d = \frac{\lambda L}{a} \qquad (1)$$

Where L is the distance between the fibre and the screen, a is the distance from the centre of the first maximum of the diffraction pattern to the first minimum, and λ is the wavelength of the light. Optical diffraction has been used to determine the cross-sectional shape and areas of iPP and iPP/TiO_2 nanocomposite fibres with extrusion speed 50 m/min. Optical diffraction pattern of these fibres was produced on a screen using a He–Ne laser beam. Fig. 2(a-e) shows the diffraction pattern of undrawn iPP fibres and iPP/TiO_2 nanocomposite fibres at different positions along the axis. Figure 3(a-e) presents the obtained cross sections of iPP and iPP/TiO_2 nanocomposite fibres at different positions along the axis. From the obtained results of cross sectional shapes, it is found the iPP/TiO_2 nanocomposite fibres have a circular shape but with different areas. In iPP fibre, the cross-sectional area is constant at different positions along the fibre axis. But iPP/TiO_2 nanocomposite fibres cross-sectional areas are unequal along the fibre axis from region to another. Table 2 gives the cross-sectional area of iPP and iPP/TiO_2 nanocomposite fibres along the fibres axis. The variations in the cross sectional areas of

nanocomposites could be due to the inconsistent distribution and agglomeration of TiO_2 nanoparticles inside and along the iPP matrix.

In order to understand the effect of TiO_2 nanoparticles in iPP/TiO_2 nanocomposite fibres, the optical properties of iPP blank fibres are investigated. A filament of iPP fibres is placed in the mechanical drawing device and immersed in a liquid of refractive index of 1.493 at temperature 24^oC (room temperature). The optical setup of the Mach-Zehnder interferometer combined with the drawing device was adjusted to obtain the two- beam interference microinterferogram. The object stage was used to move the position of the fibre 2mm along the fibre axis. An instant microinterferogram of iPP fibres was recorded accordingly using the CCD camera when the light vector vibrates parallel and perpendicular directions with the fibre axis. Then, the iPP fibre is stretched to draw ratio 1.5 and the object stage was used to move to alter the position of the fibre by 2mm along fibre axis. Figure 4 (I, II) shows a selection of the recorded microinterferograms of undrawn iPP (Fig. 4-I) and drawn iPP of draw ratio 1.5 at different positions along the fibre axis (Fig. 4-II) in the case of light vibrates parallel to the fibre axis. It is clear that the fringe shift along the fibre axis both in the drawn and undrawn iPP fibres are steady as there are no variations in the fibre thickness along the iPP fibres in both drawn and undrawn samples. This is confirmed by the diffraction measurements (Fig. 3).

Three samples of iPP/TiO_2 nanocomposites with different extrusion speeds 25 m/min, 50 m/min, and 78 m/min were opto-mechanically investigated using same as the iPP blank fibres but the refractive index of the immersion liquid in this case has changed to 1.500 at temperature 24^oC. A filament of iPP/TiO_2 nanocomposite fibre with extrusion speed 25 m/min is fixed in the mechanical drawing device which transferred to join the Mach-Zehnder interferometer. The object stage was moved 2mm along the fibre axis to alter the scanned section. The CCD camera was used to record static microinterferograms at each position along the fibre axis. After that the mechanical device was run to stretch of iPP/TiO_2 nanocomposite fibre to draw ratio of 1.5. The object stage was moved 2mm away along the fibre axis and the corresponding microinterferograms of stretched iPP/TiO_2 nanocomposite sample were recorded accordingly. The process is repeated with the other two samples of iPP/TiO_2 nanocomposites fibre. Figure 5(I, II, III) gives a selection of the recorded microinterferograms for iPP/TiO_2 nanocomposite fibres at different positions along the fibre axis in the case of light vibrates parallel to the fibre axis. Figures 5I, 5II and 5III (a-f) refer to the iPP/TiO_2 nanocomposite fibre with extrusion speeds 25 m/min, 50 m/min and 78 m/min, respectively.

Figure 6 (I, II, III) shows another selection of the recorded microinterferograms of iPP/TiO_2 nanocomposite fibre with draw ratio 1.5 at different positions (a-f) along the fibre axis in the case of light vibrates parallel to the fibre axis. Little variations in the fibre diameter were noticed at different positions along the fibre axis for each undrawn sample (see Fig. 5). But significant variations were observed in the case of drawn samples (Fig. 6) at certain positions along the fibre axis, in particular samples with low extrusion speeds (I and II). The caused deformation (e.g. necking) during the fibre drawing process, the agglomeration and clustering of TiO_2 nanoparticles along the fibre axis were the reason behind the variation obtained in the fibre thickness and its fringe shift. This is also confirmed by the diffraction measurements (Fig. 3). In other words there is diffused variations in the fringe shift along the nanocomposites in the case of the undrawn sample (Fig. 5) but in case of the drawn nanocomposite sample (Fig. 6), the fringe shifts experienced some thinning and necking deformations along the fibre axis.

For measuring the refractive indices of iPP and iPP/TiO_2 nanocomposites, an image analysis software program [reference] was used to obtain the phase map for each microinterferogram using MAT Lab environment. From which the refractive indices were calculated using the following equation [11].

$$n^{||} = n_L + \varphi\, \lambda/2\pi\, t \qquad (2)$$

Where $n^{||}$, is the refractive index when the incident light vibrates parallel to the fibre axis, n_L is the refractive index of the immersion liquid, φ is the phase difference, λ is the wavelength of the incident light, t is the thickness of the fibre. An analogue formula, for determining $n^{\perp}$, was used when light vibrates perpendicular to the fibre axis. Figure 7 (I, II) gives the variation of refractive index at different position along the fibre axis for iPP and iPP/TiO_2 nanocomposites fibres when the polarized light vibrates parallel (Fig 7-I) and perpendicular (Fig 7-II) to the fibre axis, respectively. It is clear that there are no variations in the values of refractive indices in case of parallel and perpendicular direction of the vibrating light at different position along iPP fibre axis (see figure 7 I(a) and 7 II(a)). Figures 7 I(b) and 7 II(b) showed that there is slight changes in the refractive indices of iPP/TiO_2 nanocomposite fibre in the case of extrusion speed 25m/min. Significant variations obtained in the refractive indices at different positions along the iPP/TiO_2 fibre axis in the case of extrusion speeds 50m/min and 78m/min as shown in figures 7 I(c, d) and 7 II(c, d). It is known that the addition and dispersion of nanoparticles such TiO_2 into iPP fibres could enhance some of the polymer intrinsic properties [1] and affect other

properties such as the thickness uniformity and consistency the refractive indices along the nanocomposite fibres due to the random distribution and aggregation of TiO_2 inside the fibres. . In addition the The iPP blank fibre exhibited a homogenous structure compared to the iPP/TiO_2 nanocomposite fibres

Figure 8 (I, II) gives the variation of refractive indices at different position along the fibre axis for iPP and iPP/TiO_2 nanocomposites fibres mechanically drawn at draw ratios 1.5 when incident polarized light vibrates parallel and perpendicular to the fibre axis respectively. In figure 8 I(a), a uniform increase in the values of refractive index in the parallel direction and in figure 8 II(a), a uniform decreasing in the values of refractive index in the perpendicular direction at different position along the fibre axis, respectively, due to drawing process. In figure 8 I(b, c, d) the refractive index of iPP/TiO_2 increases randomly in the parallel direction along the fibre axis. In the perpendicular direction, figure 8 II(b, c, d), irregular decrease was noticed in the refractive index along the fibre axis. The irregularities in the values of refractive indices of iPP/TiO_2 nanocomposites fibres at different position could be due to inconsistent diffusion of TiO_2 nanoparticles along the fibre axis and the elongation of the agglomerated/clustered TiO_2 during drawing process.

The birefringence is one of the trusted tools of measuring the degree of molecular orientation and anisotropic properties of polymers. Birefringence (Δn) can be calculated from the difference between the refractive indices as follows:

$$\Delta n = n^{||} - n^{\perp} \qquad (3)$$

Figure 9 (I, II) gives the variation of birefringence of iPP and iPP/TiO_2 nanocomposites fibres at different position along the fibre axis for undrawn (Fig. 9I) and drawn (draw ratio 1.5) (Fig. 9II), respectively. The birefringence gives the overall behaviour of molecular orientation including the diffusion of TiO_2 nanoparticles during drawing process. The birefringence behaviour along the fibre axis agree with the published data on nanofibers [18].

To extend our investigations of iPP/TiO_2 nanocomposites fibres, the optical properties were measured across the fibre diameter. The refractive index profile taking the refraction of the incident light beam inside the fibre into consideration was determined using the following equation [19-22]:

$$\frac{\lambda\varphi_Q}{2\pi} = \sum_{j=1}^{Q-1} 2n_j \left[\sqrt{[(R-(j-1)a]^2 - \left(d_Q n_L/n_j\right)^2]} - \sqrt{(R-ja)^2 - \left(d_Q n_L/n_j\right)^2}\right]$$
$$+ 2n_Q\sqrt{[(R-(Q-1)a]^2 - \left(d_Q n_L/n_Q\right)^2}$$
$$- n_L\left[\sqrt{R^2-d_Q^2} + \sqrt{R^2-x_Q^2}\right] \qquad (4)$$

Where R is the fibre radius, j is the layer number, Q is the number of layers, a is the thickness of each layer (a = R/Q), n_j is the refractive index of the layer jth, d_Q is the distance between the incident beam and the centre of the fibre, x_Q is the distance between the emerging beam and the centre of the fibre and φ_Q is the the phase difference corresponding to the point x_Q and λ is the wavelength of the incident light. Figures 10 and 11 illustrate the refractive index profiles along the fibre axis when polarized light vibrates parallel and perpendicular to the fibre axis for iPP fibres and iPP/TiO_2 nanocomposite fibres with extrusion speeds 25 m/min, 50 m/min, and 78 m/min. These figures indicate homogenous structure of iPP fibres (Figs 10(a),11(a)). Figures 10(b) and 11(b) show the refractive index profile for iPP/TiO_2 nanocomposite fibres with extrusion speed 25 m/min in the parallel and perpendicular directions, respectively. In these figures the refractive index increased gradually from the fibre surface towards the centre of the sample but its value changes along the fibre axis. Figures 10(c) and 11(c) show the refractive index profile for iPP/TiO_2 nanocomposite fibres with extrusion speed 50 m/min in the parallel and perpendicular direction, respectively. In the parallel direction, the values of the refractive index profile tend to be constant at 2, 6, 10 and18 mm and the structure is nearly homogeneous but at 14mm a skin-core structure was obtained. In Figure 10 (c) at 22 mm the values of the refractive index profile suddenly increased and jumped over the other profiles along the fibre axis. In the perpendicular direction (Fig. 11) the values of the refractive index profile decreased gradually on going from the fibre surface towards the centre except at 22 mm the values of the refractive profile increased and jumped to the top compared to the other profiles. Figures 10(d) and 11(d) shows the refractive index profile for iPP/TiO_2 nanocomposites fibres with extrusion speed 78 m/min in the parallel and perpendicular direction, respectively. Same behaviour obtained as the values of the refractive profile increased gradually on going from the fibre surface towards the centre along on the fibre axis (Fig 10(a)). In figure 11(d) the values of the refractive profile decreased gradually on going from the fibre surface towards the centre along the fibre axis and some irregular increment in the values of diameter of the fibre were also noted.

Figures 12 and 13 show the refractive index profiles of drawn iPP and iPP/TiO_2 nanocomposite fibres with different extrusion speeds 25 m/min, 50 m/min, and 78 m/min at different position along the fibre axis at draw ratio 1.5. The incident polarized light vibrates in parallel (Fig. 12) and perpendicular (Fig. 13) to the fibre axis, respectively. The values of the refractive profile in parallel direction increased gradually (Fig. 12(a)), and gradually decreased in the perpendicular direction (Fig. 13(a)) at different positions along the iPP fibre axis. The refractive index profile for the three samples of iPP/TiO_2 nanocomposite fibres at draw ratio D=1.5 gradually increased in some regions and stable at others in the parallel direction. They increased at 2, 6, 14 and 24mm (Fig. 12(b)) and 4, 22, 24mm (Fig. 12(c)) along the fibre axis. They are stable at 12 mm (Figs 12 (b)) and at 10, 14 and 18mm (Fig.12(c)) along the fibre axis. The refractive index profiles for the same samples are found to be gradually decreased in the perpendicular direction (Fig. 13), they decreased at regions 2, 6, 14 and 24mm along the fibre axis. Figures 12 and 13 illustrated that, the refractive index profiles of iPP fibres have regular (homogeneous) structure. While the profiles of iPP/TiO_2 nanocomposite exhibited irregular changes along the fibre axis due to of irregular distribution of TiO_2 nanoparticles inside the iPP fibre blank fibre. It is also noted that the value of fibre diameter has fluctuating up (increase) and down (decrease) along the fiber axis. In general the inconsistent values of fibre diameter and refractive indices of the iPP/TiO_2 nanocomposites along the fibre axis and across the fibre diameter could be due to the lack of well distribution of TiO_2 nanoparticles during manufacturing and cold drawing process.

5. Conclusions

The Mach–Zehnder interferometer is proven to be a capable technique to investigate the opto-mechanical properties of iPP/TiO_2 nanocomposite fibres with different extrusion speeds and at different draw ratios. The micro-interferograms obtained have qualitatively identified the differences in the fibre thickness and optical path variations along the fibre axis. As the draw ratio increases the birefringence increases leading to an increase in the molecular orientation that impacted the stiffness and ductility of iPP/TiO_2 nanocomposites during the cold drawing. The refractive index and birefringence profiles for iPP and iPP/TiO_2 nanocomposite fibres at different draw ratio indicates that these fibres are homogenous in structure in some regions and not in others as a skin-core structure along the fibre axis has been also predicted. The inconsistent variation in both fibre diameter and refractive indices of the iPP/TiO_2

nanocomposites along and across the fibre axis refer to the irregular distribution of TiO_2 nanoparticles during manufacturing and cold drawing process.

Acknowledgements

The authors would like to express their appreciation to professor A. A. Hamza Professor of Physics, X-president of Mansoura University for his valuable discussion and kindly support during this work.

References

1. El-Dessouky HM, Lawrence CA. Nanoparticles dispersion in processing functionalised PP/TiO2 nanocomposites: Distribution and properties. J. Nanoparticle Res. 2011;13:1115-1124.
2. Magniez K. Development of novel melt-spun nanocomposite fibers. SPE Plastics research online. 2011 http://www.4spepro.org/index.php
3. Schadler LS, Brinson LC, Sawyer WG. Polymer Nanocomposites:A Small Part of the Story. J. of the Minerals, Metals & Materials Society. 2007;59:53-60
4. Serrano C, Cerrada ML , García MF, Ressia J, Vallés EM. Rheological and structural details of biocidal iPP-TiO2 nanocomposites. J. Europ. Polym. 2012; 48:586–596
5. Esthappan SK. Polypropylene/metal oxide nanocomposites: fibre spinning and evaluation. PhD thises. Cochin Univ of Sci and Tech India .2012
6. Ohama Y, Gemert DV. Application of titanium dioxide photocatalysis to construction materials. Springer Dordrecht Heidelberg London New York,2011
7. Erdem N, Erdogan UH, Cireli AA, Onar N. Structural and Ultraviolet-Protective Properties of Nano-TiO2-Doped Polypropylene Filaments. J. Appl. Polym. Sci. 2010;115:152–157.
8. Madani M. Mechanical Properties of Polypropylene Filled with Electron Beam Modified Surface-treated Titanium Dioxide Nanoparticles. J of Reinforced Plastics and Composites. 2010; 29:1999 -2014.
9. Serrano C, Cerrada ML, García MF, Ressia J and Vallés E M . Rheological and structural details of biocidal iPP-TiO2 nanocomposites. European Polym. J.2012; 48 : 586–596
10. Chiu CW , Lin CA, Hong PD. Melt-spinning and thermal stability behaviorof TiO2 nanoparticle/polypropylene nanocomposite fibers. J Polym Res. 2011; 18:367–372
11. Barakat N, Hamza AA. Interferometry of Fibrous Materials, Bristol: Adam Hilger, NewYork, 1990

12. Hamza AA, Belal AE, Sokkar TZN, El-Bakary MA, Yassien KM. Interferometric detection of structure deformation due to cold drawing of polypropylene fibres at high draw ratios. J of Opt. A: Pure Appl. Opt. 2007; 9: 820–827
13. Sokkar TZN, El – Farahaty KA, El-Bakary MA, Raslan MI, Omar EZ, Hamza AA. Non-interferometric determination of optical anisotropy in highly-oriented fibres using transport intensity equation technique. Optics and Lasers in Engineering. 2018; 102:10-16
14. El-Bakary MA. The effect of mechanical drawing on optical and structural properties of nylon 6 fibres. Optics & Laser Technology. 2007; 39 : 1273-1280
15. Andrew JM, Ward IM. The Cold-Drawing of High Density Polyethylene Mater Sci 1970; 5: 411-417
16. Curry SM, Schawlow AL. Measuring the diameter of a hair by diffraction", American Journal of Physics,1974;42:412-413.
17. Sokkar TZN, El-Bakary MA. Determination of the refractive index of fibres using the modified area method: I. Homogeneous fibres. Optics & Laser Technology. 2004; 36:507-513
18. Kołbuk D, Sajkiewicz P, Tomasz A. Kowalewski. Optical birefringence and molecular orientation of electrospun polycaprolactone fibres by polarizing-interference microscopy. J. Europ. Polym. 2012; 48:275-283
19. Hamza AA, Sokkar TZN, Ghander AM, Mabrouk MA, Ramadan WA. On the determination of the refractive index of a fibre II. Graded Index Fibre. Pure Appl Opt. 1995; 4:161–177.
20. El-Bakary MA. Determination of Refractive Index Profile of Partially and Highly Oriented Fibres Using Double Refracting Interference Microscopy. J. Appl. Polym. Sci. 2003; 87:2341-2347
21. Sokkar, TZN, El-Farahaty KA, El-Bakary MA, Omar EZ, Agour M, Hamza, AA.Adaptive spatial carrier frequency method for fast monitoring optical properties of fibres. Appl. Phys. B. 2016; 5: 122-138.
22. Sokkar TZN, El-Bakary MA, Ali AM. The Influence of Mechanical Cold Drawing and Drawing Velocity on the Molecular Structure of Isotactic Polypropylene Fiber. J.Appl .Polym. sci. 2012

Figures captions

Figure (1): Schematic diagram of the optical system used (Mach – Zehnder interferometer) where; S is spatial filter, P is Polarizer, BS1 and BS2 are two identical beam splitters, M1 and

M2 are two identical mirrors, OS is objective stage, MO is microscope objective and CCD is Charged coupled device (camera).

Figure (2): Diffraction patterns of iPP and iPP/TiO_2 nanocomposite fibres with extrusion speed 50m/min at different position along the fibre axis respectively, using He-Ne laser beam of wavelength $\lambda = 632.8$ nm at distances a) 1 cm, b) 2 cm, c) 3 cm, d) 4 cm and e) 5 cm

Figure (3): The graphical representation of cross-sectional areas of iPP and iPP/TiO_2 nanocomposite fibres at different position along the fibre axis; a) 1 cm, b) 2 cm, c) 3 cm, d) 4 cm and e) 5 cm

Figure (4): Microinterferograms of iPP fibres in the case of the polarized light vibrates in parallel direction to the fibre axis. I) iPP fibre and II) drawn iPP fibre at draw ratio 1.5 at different position along the fibre axis: a) 0 mm, b) 4 mm, c) 8 mm, d) 12 mm, e) 16 mm and f) 20 mm

Figure (5): Microinterferograms of undrawn iPP/TiO_2 nanocomposites fibres when the incident polarized light vibrates in parallel direction to the fibre axis with extrusion speeds I) 25 m/min, II) 50 m/min and III) 78 m/min along to the fibre axis: a) 0 mm, b) 4 mm, c) 8 mm, d) 12 mm, e) 16 mm and f) 20 mm

Figure (6): Microinterferograms of extruded iPP/TiO_2 nanocomposites fibres at draw ratio 1.5 when the incident polarized light vibrates in parallel direction to the fibre axis with extrusion speeds I) 25 m/min, II) 50 m/min and III) 78 m/min along to the fibre axis: a) 0 mm, b) 4 mm, c) 8 mm, d) 12 mm, e) 16 mm, f) 20 mm

Figure 7: The refractive indices ($n^{\parallel}$ and $n^{\perp}$) of iPP (a) and iPP/TiO_2 nanocomposite fibres with extrusion speeds 25 m/min (b), 50 m/min (c), and 78 m/min (d) along the fibre axis.

Figure 8: The refractive indices ($n^{\parallel}$ and $n^{\perp}$) of iPP (a) and drawn iPP/TiO_2 nanocomposite fibres with extrusion speeds 25 m/min (b), 50 m/min (c), and 78 m/min (d) along the fibre axis at draw ratio 1.5.

Figure 9: The birefringence of iPP (a) and iPP/TiO_2 nanocomposite fibres with extrusion speeds 25 m/min (b), 50 m/min (c), and 78 m/min (d) along the fibre axis. I) undrawn and II) at draw ratio 1.5

Figure 10: The refractive index profile of iPP (a) and iPP/TiO_2 nanocomposite fibres with extrusion speeds 25 m/min (b), 50 m/min (c), and 78 m/min (d) along the fibre axis when the incident light polarized in parallel direction.

Figure 11: The refractive index profile of iPP (a) and iPP/TiO_2 nanocomposite fibres with extrusion speeds 25 m/min (b), 50 m/min (c), and 78 m/min (d) along the fibre axis when the incident light polarized in perpendicular direction.

Figure 12: The refractive index profile of iPP (a) and iPP/TiO_2 nanocomposite fibres with extrusion speeds 25 m/min (b), 50 m/min (c), and 78 m/min (d) along the fibre axis when the incident light polarized in parallel direction at draw ratio 1.5.

Figure 13: The refractive index profile of iPP (a) and iPP/TiO_2 nanocomposite fibres with extrusion speeds 25 m/min (b), 50 m/min (c), and 78 m/min (d) along the fibre axis when the incident light polarized in perpendicular direction at draw ratio 1.5.

Table (1): Extrusion speed and average diameter of iPP/TiO_2 nanocomposite (iPP+2%TiO_2) monofilaments.

iPP/TiO_2 nanocomposites	Extrusion speed	Average diameter (μm)
Sample (1)	25m/min	257
Sample (2)	50m/min	188
Sample (3)	78m/min	92

Table (2): The cross-sectional area of iPP and iPP/TiO_2 nanocomposite fibres along the fibre's axis.

Distance along the fibre axis (cm)	cross-sectional area in unit (μm^2) ×10^2			
	iPP	iPP/TiO_2 (25 m/min)	iPP/TiO_2 (50 m/min)	iPP/TiO_2 (78 m/min)
1	92.54	524.39	320.28	83.90
2	92.54	524.39	277.91	73.74
3	92.54	561.18	231.40	65.32
4	92.54	624.06	263.68	58.27
5	92.54	581.04	301.69	65.32

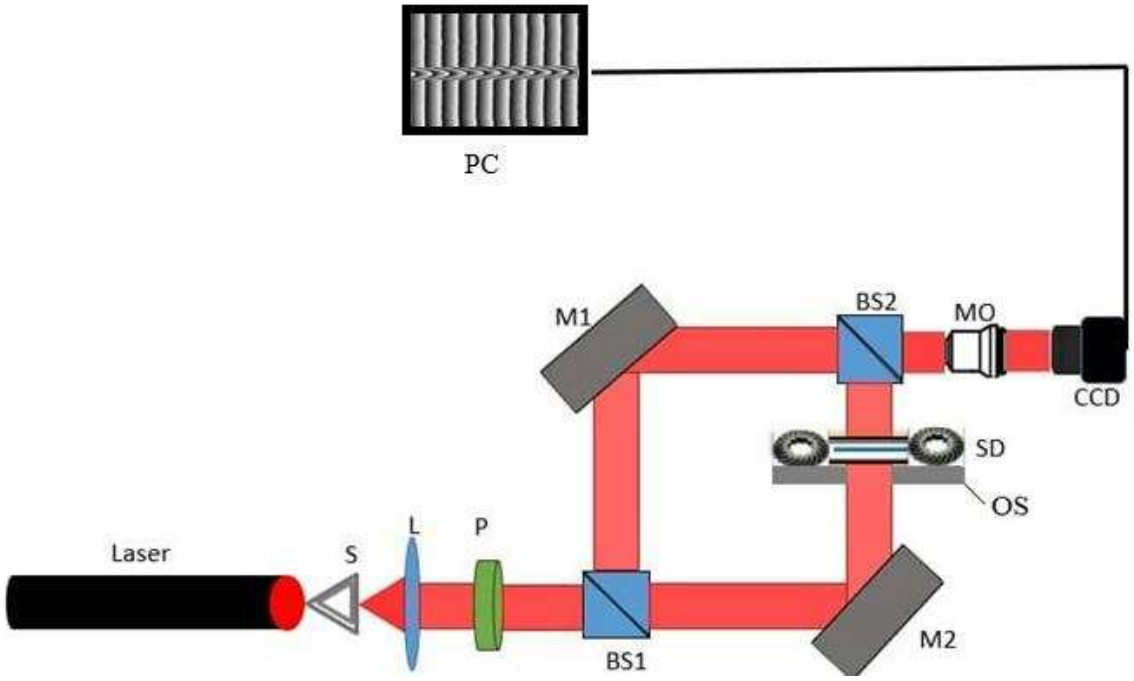

)1Figure (

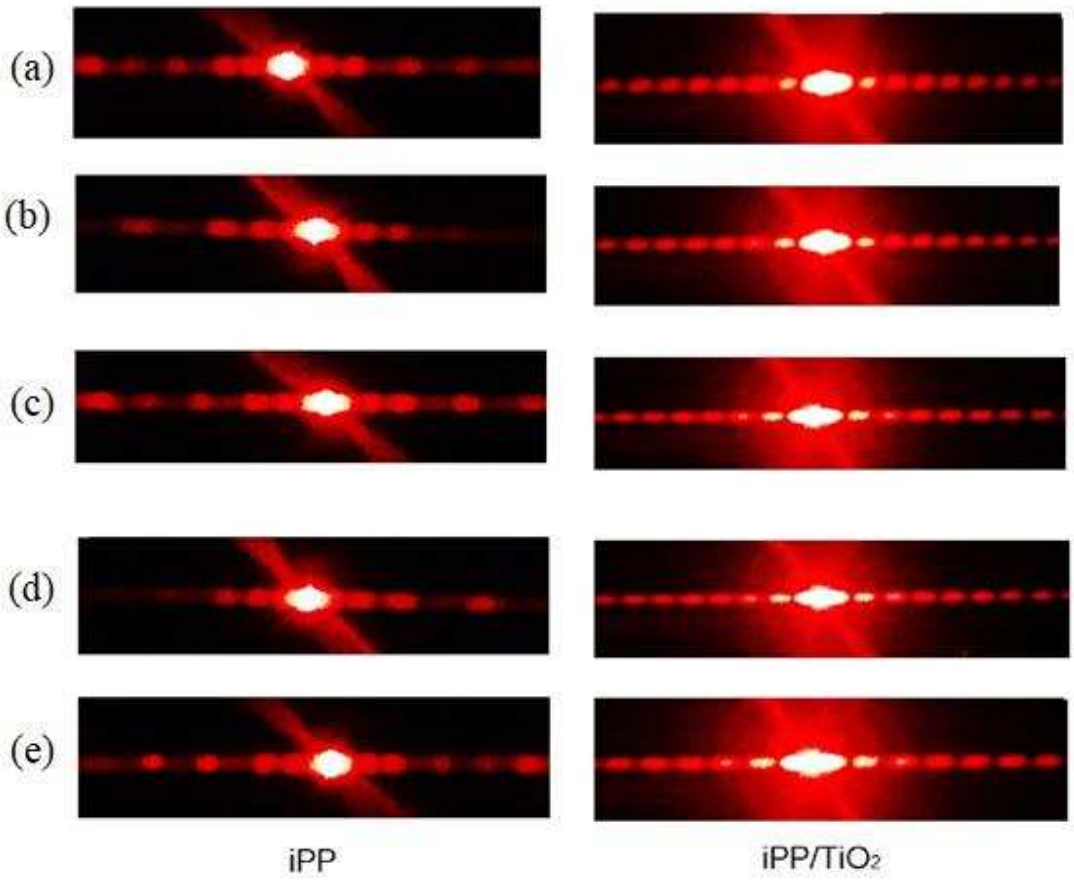

Figure (2)

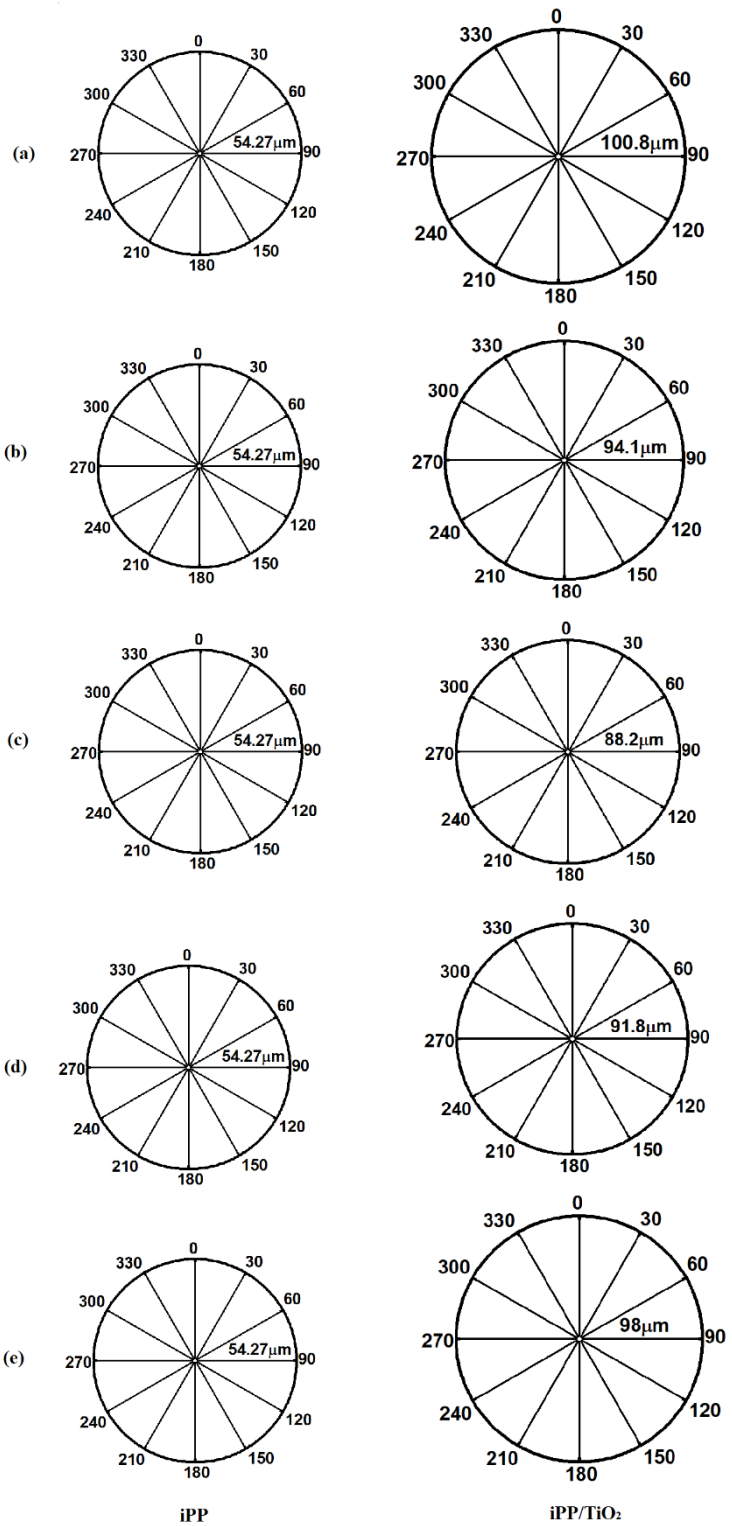

Figure (3)

(I) (II)

(a)

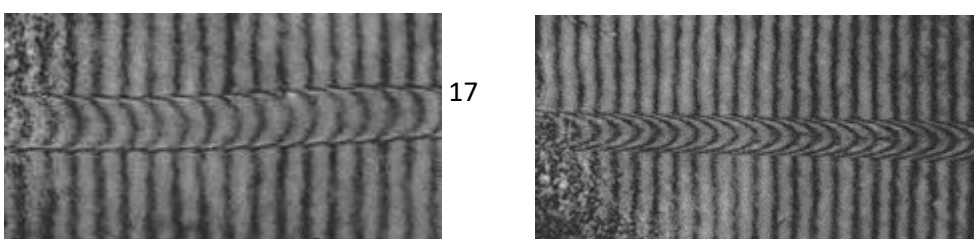

Figure (4)

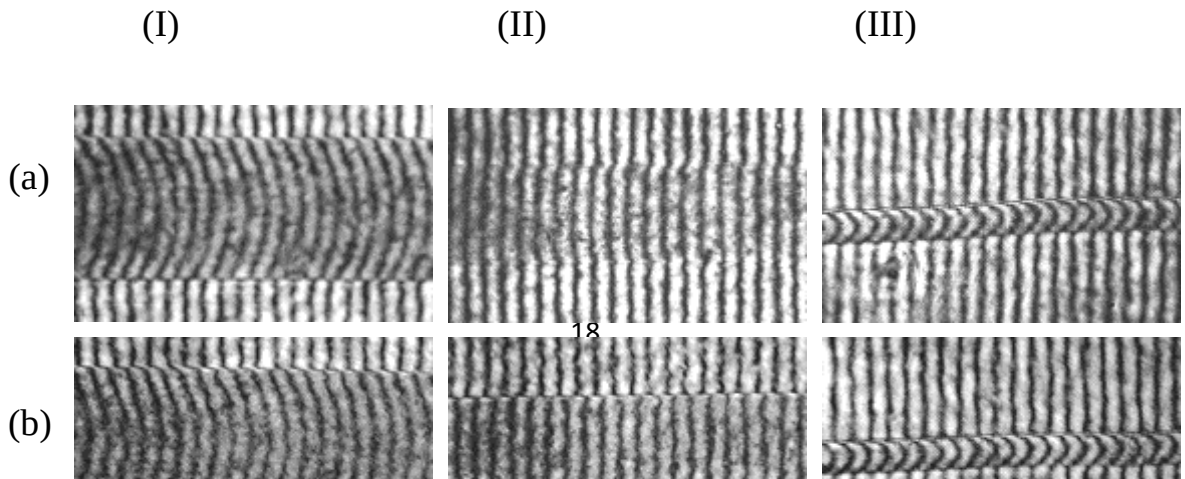

h

Figure (5)

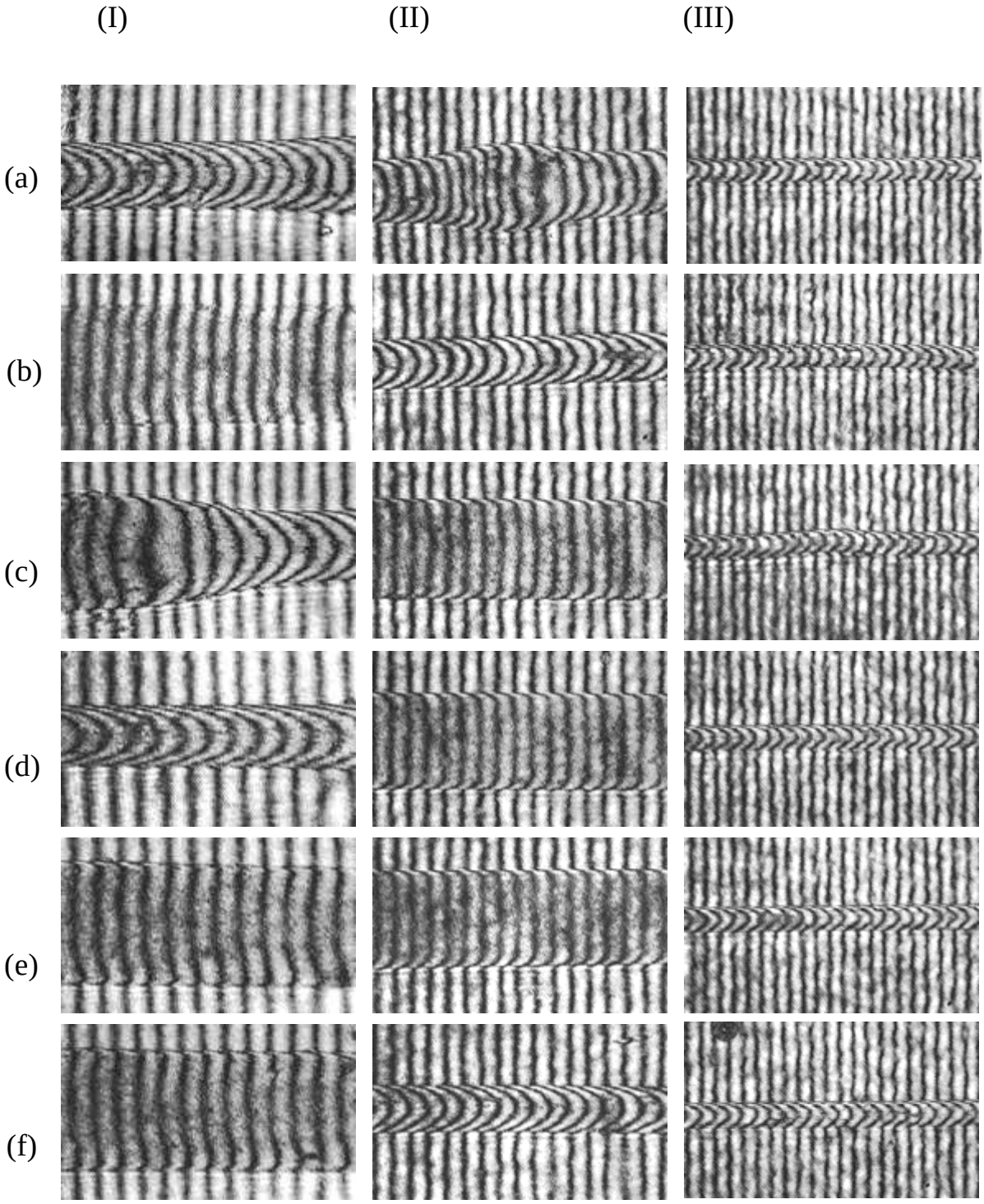

Figure (6)

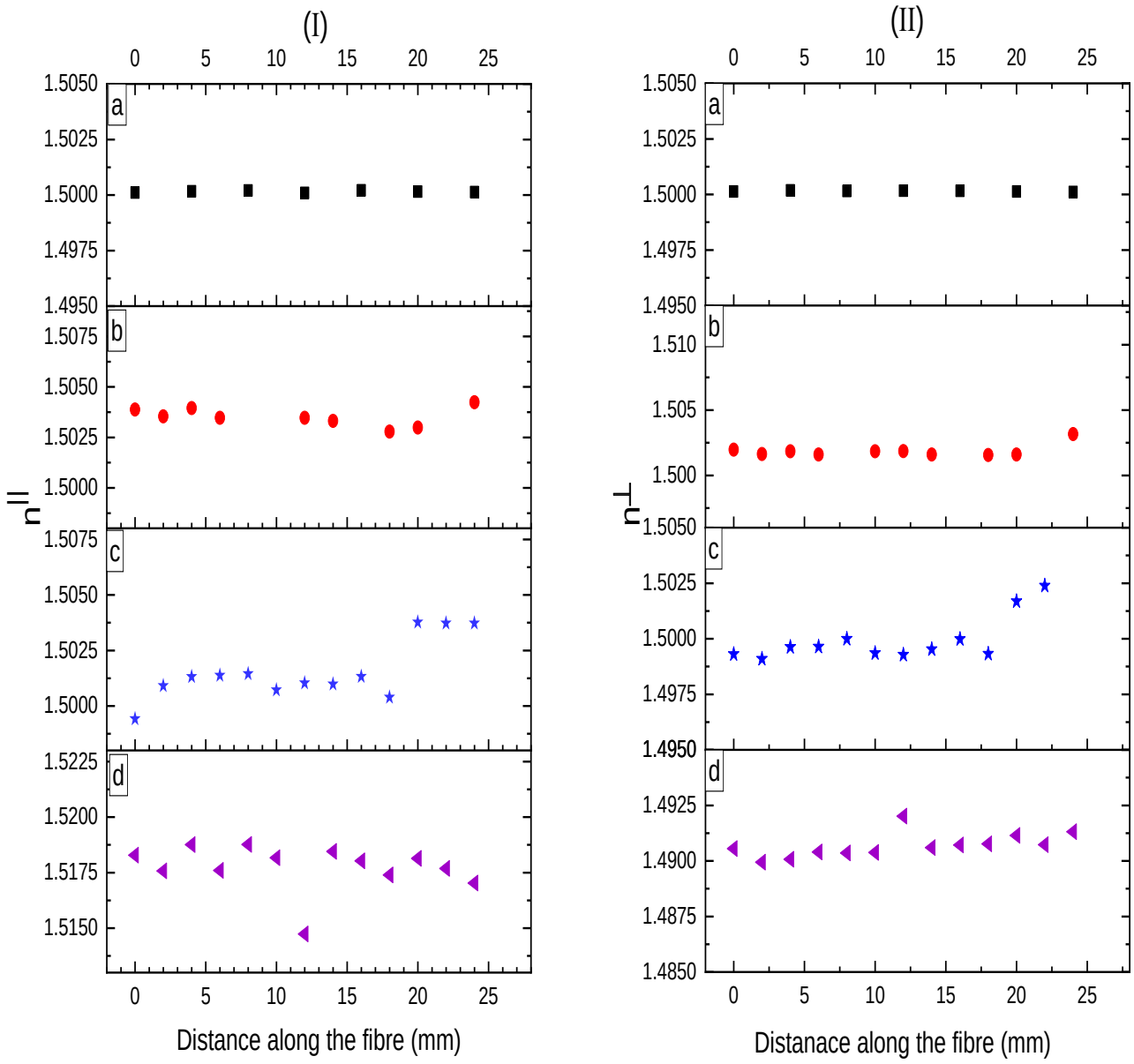
(I)
(II)
a
b
c
d
$n_{\parallel}$
$n_{\perp}$
Distance along the fibre (mm)
Distanace along the fibre (mm)

Figure (7)

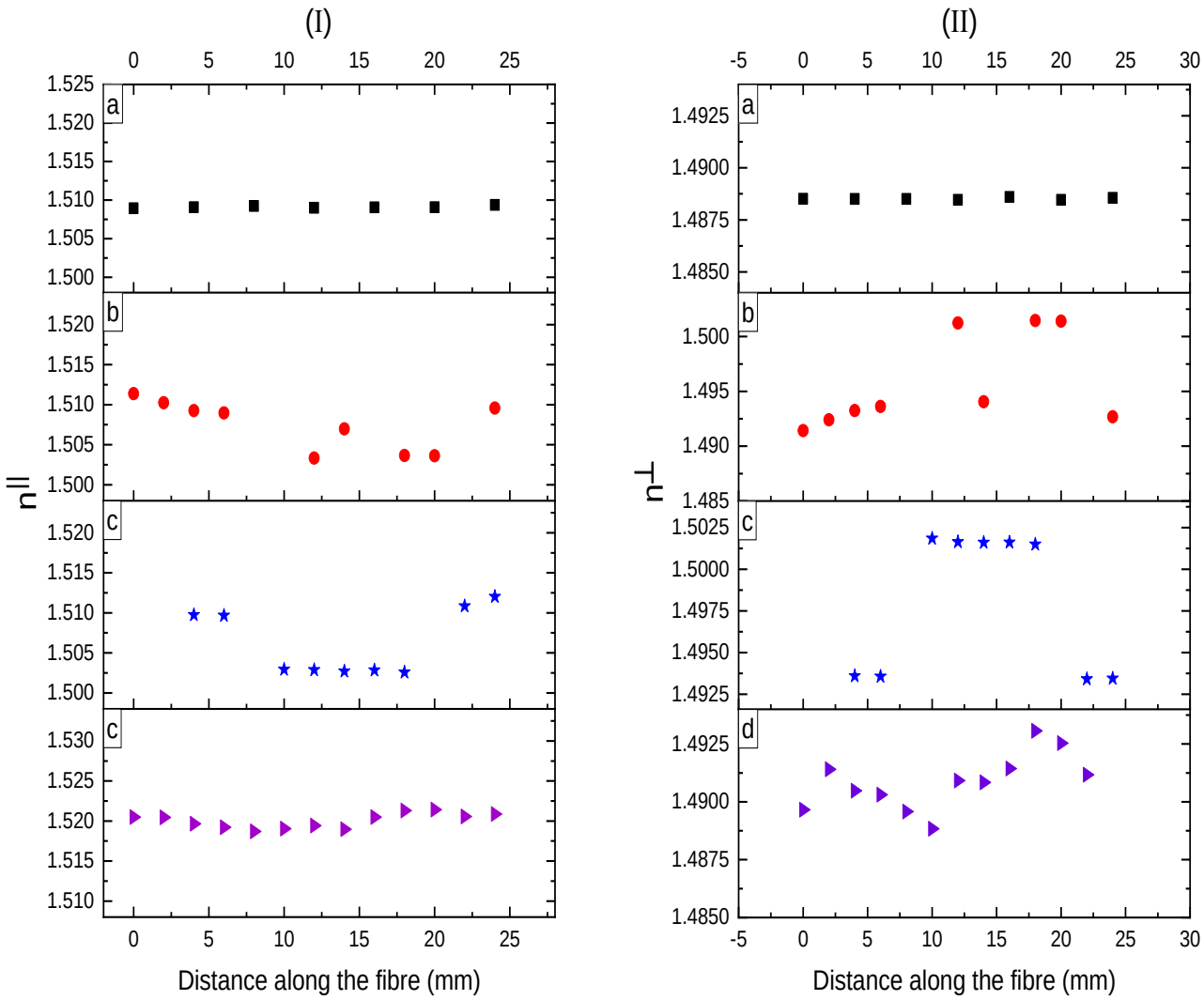
(I)
(II)
a
b
c
c
d
$n^{\parallel}$
$n^{\perp}$
Distance along the fibre (mm)
Distance along the fibre (mm)

Figure (8)

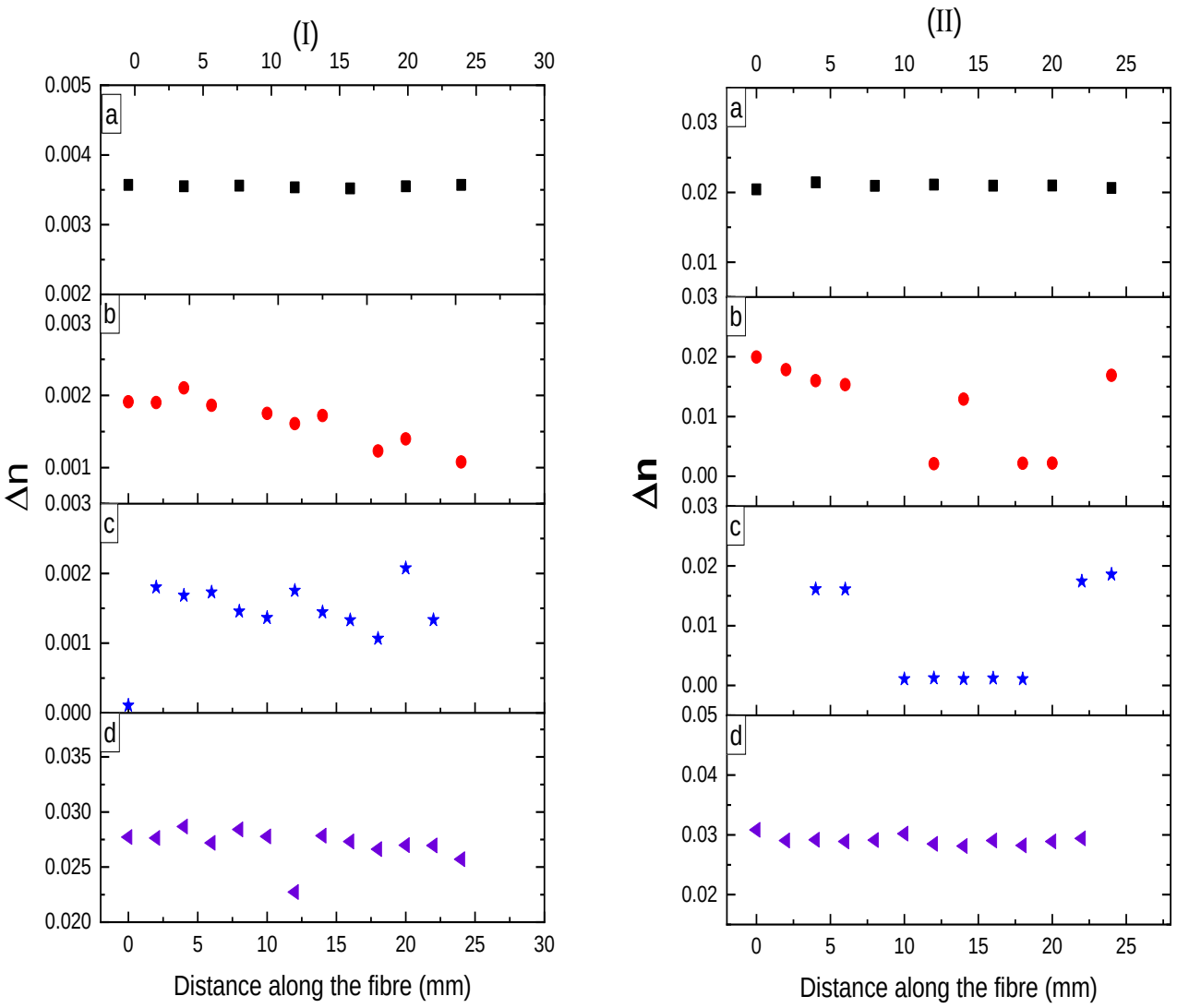
(I)
(II)
a
b
c
d
Δn
Distance along the fibre (mm)
Distance along the fibre (mm)

Figure (9)

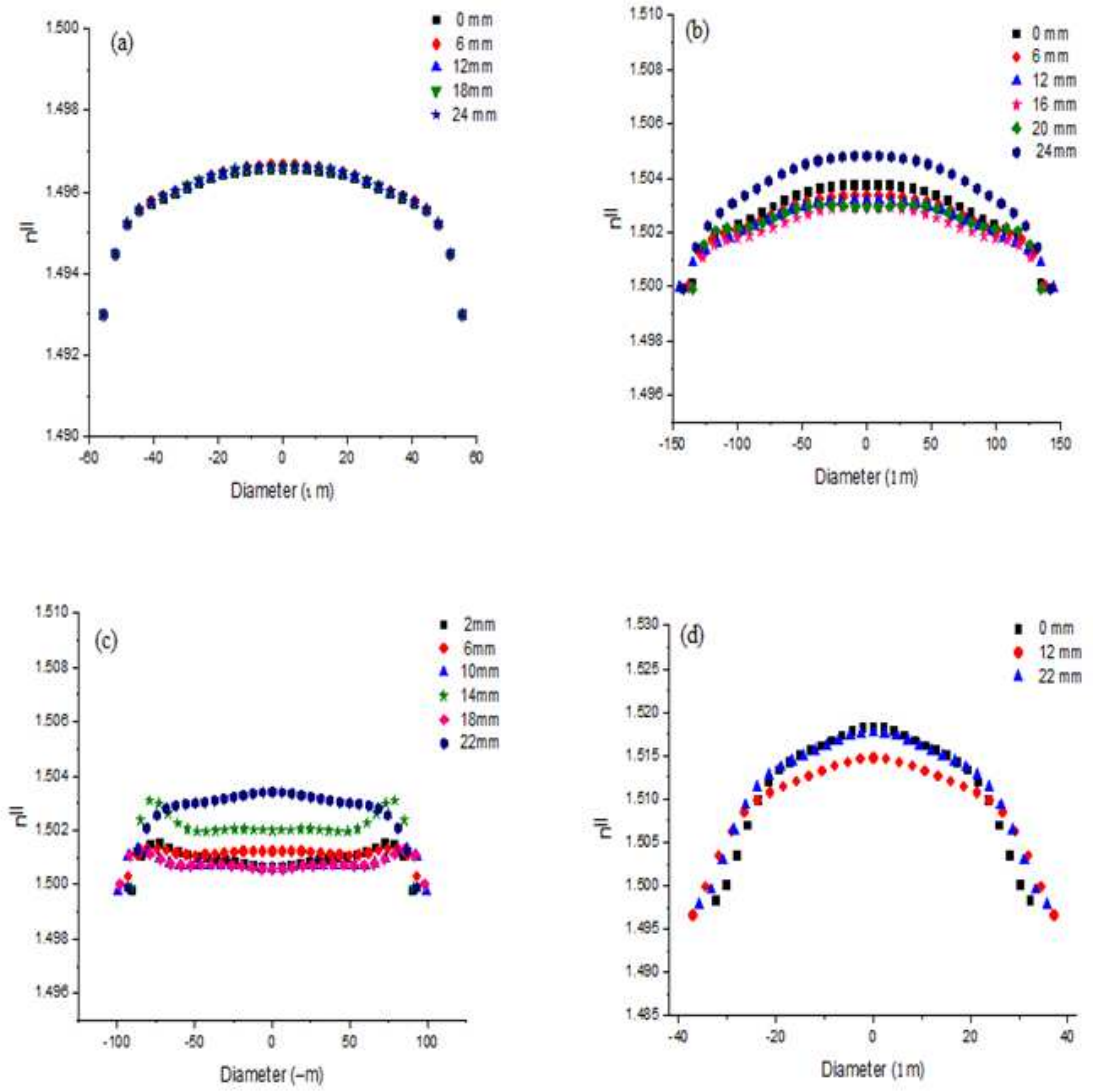
(a)
0 mm
6 mm
12mm
18mm
24 mm
n||
Diameter (1 m)
(b)
0 mm
6 mm
12 mm
16 mm
20 mm
24mm
n||
Diameter (1m)
(c)
2mm
6mm
10mm
14mm
18mm
22mm
n||
Diameter (–m)
(d)
0 mm
12 mm
22 mm
n||
Diameter (1m)

Figure (10)

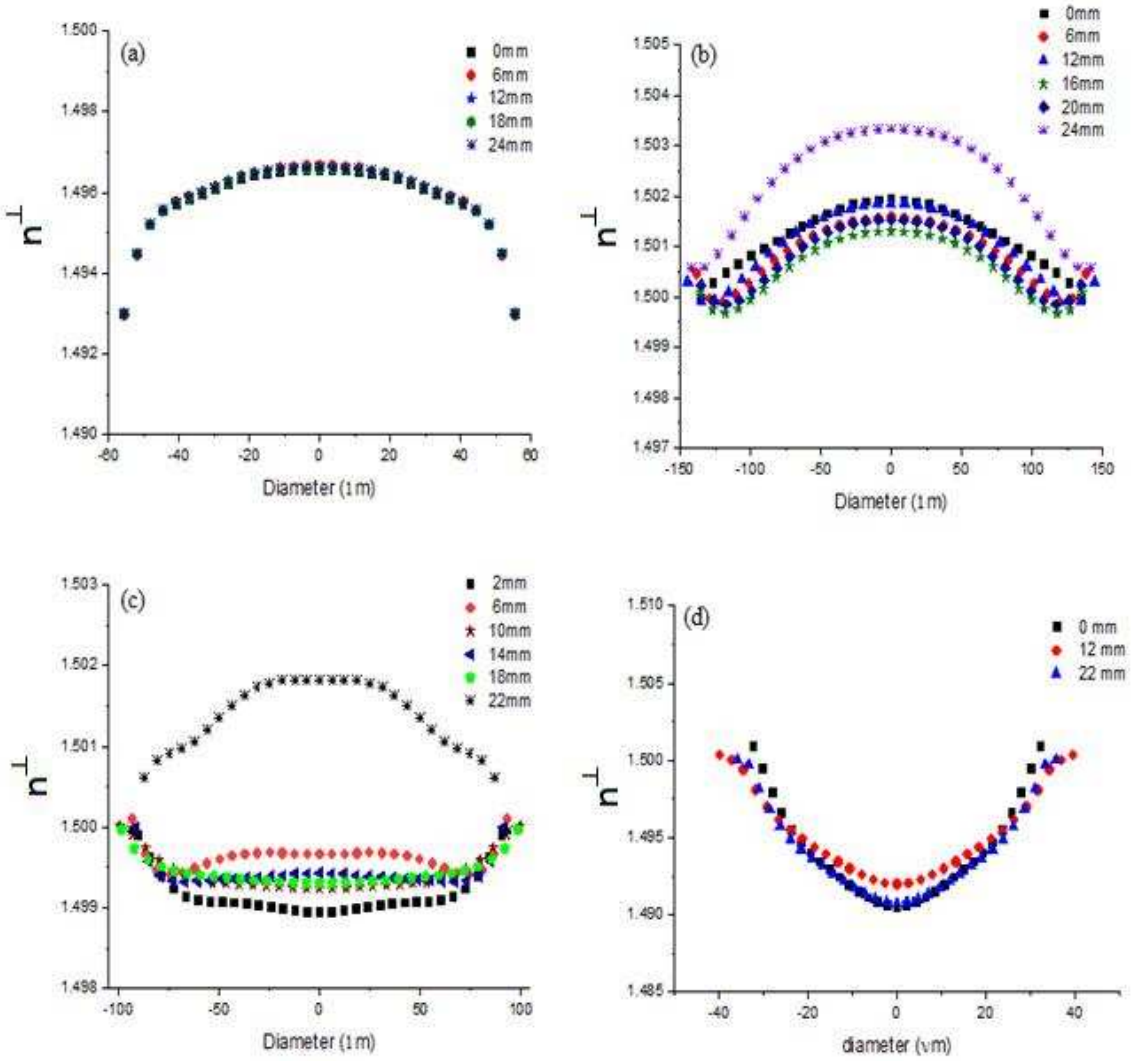
(a)
0mm
6mm
12mm
18mm
24mm
Diameter (1m)
(b)
0mm
6mm
12mm
16mm
20mm
24mm
Diameter (1m)
(c)
2mm
6mm
10mm
14mm
18mm
22mm
Diameter (1m)
(d)
0 mm
12 mm
22 mm
diameter (νm)

Figure (11)

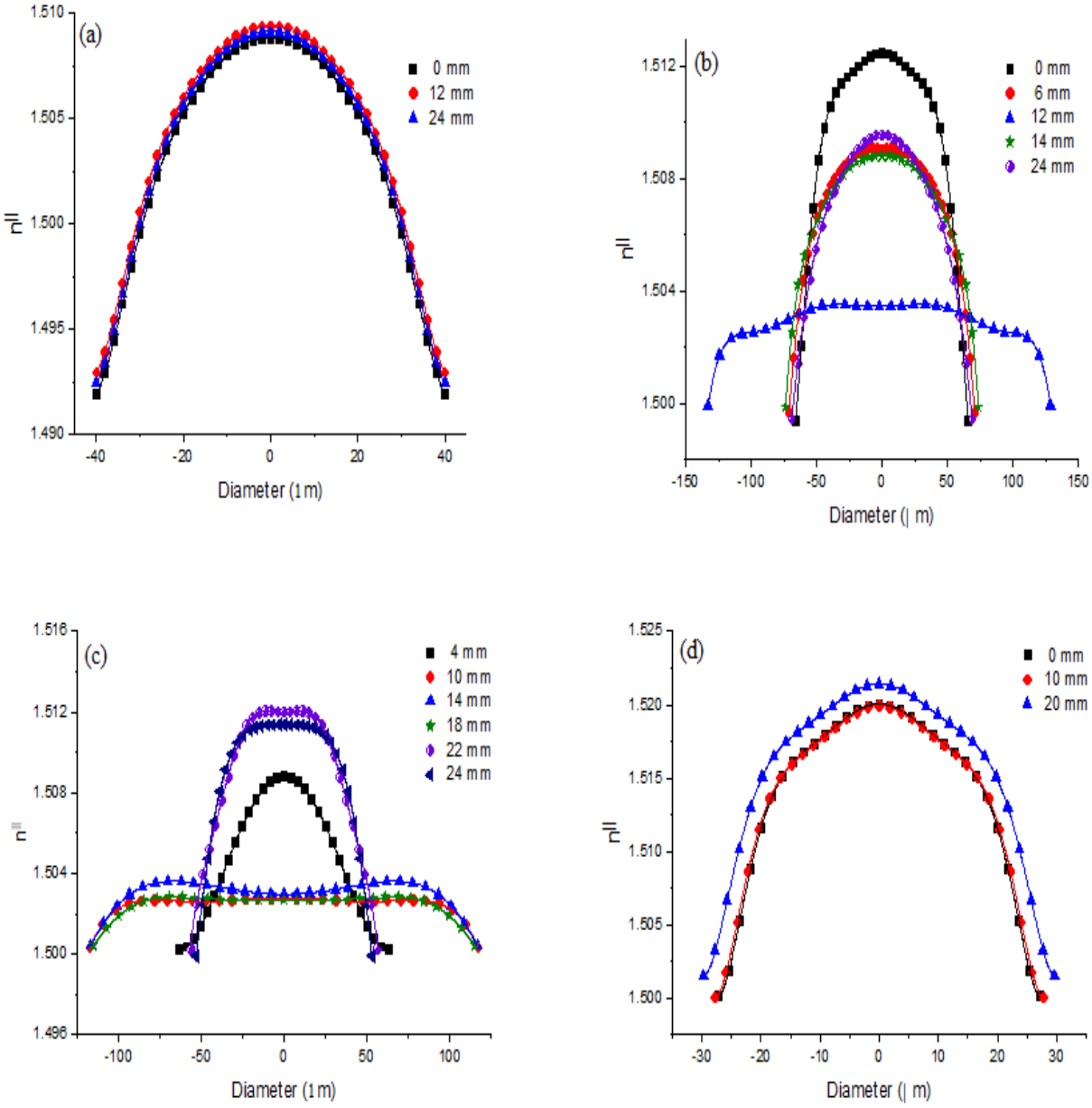
(a)
0 mm
12 mm
24 mm
n
Diameter (1 m)
(b)
0 mm
6 mm
12 mm
14 mm
24 mm
n
Diameter (| m)
(c)
4 mm
10 mm
14 mm
18 mm
22 mm
24 mm
n
Diameter (1 m)
(d)
0 mm
10 mm
20 mm
n
Diameter (| m)

Figure (12)

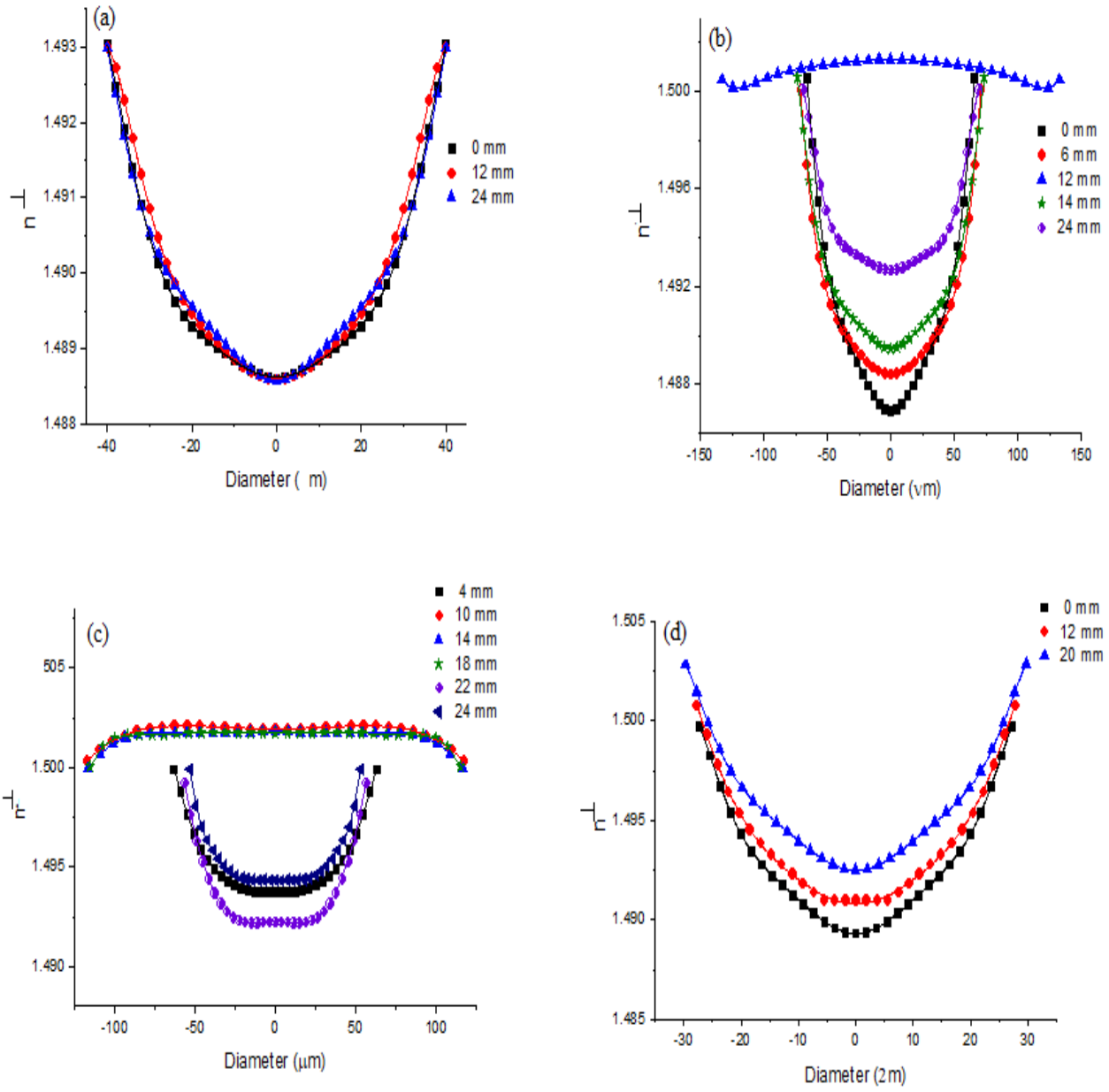
(a)
1.493
1.492
1.491
1.490
1.489
1.488
n⊥
-40
-20
0
20
40
Diameter (m)
0 mm
12 mm
24 mm
(b)
1.500
1.496
1.492
1.488
n⊥
-150
-100
-50
0
50
100
150
Diameter (νm)
0 mm
6 mm
12 mm
14 mm
24 mm
(c)
505
1.500
1.495
1.490
n⊥
-100
-50
0
50
100
Diameter (μm)
4 mm
10 mm
14 mm
18 mm
22 mm
24 mm
(d)
1.505
1.500
1.495
1.490
1.485
n⊥
-30
-20
-10
0
10
20
30
Diameter (2m)
0 mm
12 mm
20 mm

Figure (13)